Raman spectrum of CrI_3: An *ab initio* study

Daniel T. Larson
Department of Physics, Harvard University, Cambridge, Massachusetts 02138, USA

Efthimios Kaxiras
Department of Physics and John A. Paulson School of Engineering and Applied Sciences, Harvard University, Cambridge, Massachusetts 02138, USA

(Received 30 March 2018; published 3 August 2018)

We study the Raman spectrum of CrI_3, a material that exhibits magnetism in a single layer. We employ first-principles calculations within density functional theory to determine the effects of polarization, strain, and incident angle on the phonon spectra of the three-dimensional bulk and the single-layer two-dimensional structure, for both the high- and low-temperature crystal structures. Our results are in good agreement with existing experimental measurements and serve as a guide for additional investigations to elucidate the physics of this interesting material.

DOI: 10.1103/PhysRevB.98.085406

I. INTRODUCTION

The demonstration of magnetism in a single layer of CrI_3 [1] has exciting implications for the creation of novel materials and devices based on combinations of atomic layers with varied properties. CrI_3 is a layered material that can be cleaved into flakes varying in thickness from a single layer to many layers. The magnetic ordering of bulk crystals has been carefully studied both theoretically [2] and experimentally [3], demonstrating both intra- and interlayer ferromagnetic coupling with a total magnetic moment of $3\mu_B$/Cr atom. Further predictions about single layers of CrI_3 have been carried out, including a calculation of the magnetic anisotropy energy of 686 μeV/Cr by Zhang *et al.* [4], and estimates of the Curie temperature by Liu *et al.* [5]. Now that single layers of CrI_3 have been successfully produced and characterized [1], we seek to probe its material properties in greater detail. A standard, powerful technique to characterize the properties of atomically thin materials is Raman spectroscopy [6]. Although the phonon dispersion for single-layer chromium trihalides has been presented by Zhang *et al.* [4], to our knowledge the identification of Raman-active modes is absent in the literature. Motivated by the importance of Raman spectroscopy experiments, we have studied the phonon spectrum of bulk and single-layer CrI_3 in order to elucidate the dependence of the Raman spectrum on thickness, polarization, strain, and incident angle. Our results agree well with the location and polarization dependence of the Raman peaks in existing experimental measurements and serve as a guide for further studies of this intriguing material.

II. NUMERICAL METHODS

We obtain the Raman spectrum of CrI_3 using first-principles density-functional theory (DFT) calculations. In order to study the dependence of the Raman spectrum on the sample thickness, we considered periodic cells with crystallographic dimensions and cells containing a single layer separated from its periodic images in the direction perpendicular to the layer by a vacuum region of 20 Å, which eliminates interlayer interactions.

Starting from the crystallographic structure, we obtain the fully relaxed primitive cell parameters using VASP [7,8] spin-polarized calculations with projector augmented wave pseudopotentials, the Perdew-Burke-Ernzerhof exchange-correlation functional [9], a plane-wave energy cutoff of 300 eV, and a $10 \times 10 \times 10$ k-point mesh ($10 \times 10 \times 1$ for single-layer structures). Partial occupancies were handled using Gaussian smearing with a width of 0.05 eV, and van der Waals corrections were taken into account using the DFT-D3 method [10].

Using the frozen phonon method as implemented in the PHONOPY code [11], we determine the phonon frequencies and normal modes at the Γ point from the internal forces of $2 \times 2 \times 2$ ($2 \times 2 \times 1$) bulk (single-layer) supercells containing displaced atoms, with a properly scaled k-point mesh. To estimate the relative intensity of Raman scattering from each mode we calculate the derivative of the macroscopic dielectric tensor based on finite differences for cells displaced in the direction of each mode [12].

III. PHONON SPECTRUM

At room temperature CrI_3 has the monoclinic $AlCl_3$ structure type (space group $C2/m$, No. 12), but as the temperature decreases below $T \sim 220$ K it undergoes a structural phase transition to the rhombohedral BiI_3 structure type (space group $R\bar{3}$, No. 148) [3]. The crystal structure of single-layer CrI_3 is shown in Fig. 1. The bulk structure consists of stacks of the individual layers, with the primary difference between high- ($C2/m$) and low-temperature ($R\bar{3}$) structures being the alignment of the layers.

The phonon modes of CrI_3 are determined by the symmetries of the point groups associated with the high- and low-temperature structures. The irreducible representation of the point group to which each phonon mode belongs determines whether or not it is Raman active. For the high-temperature ($C2/m$) structure the point group is C_{2h} which has four one-dimensional irreducible representations, labeled A_g, B_g, A_u, and B_u. The A_g and B_g representations have even parity

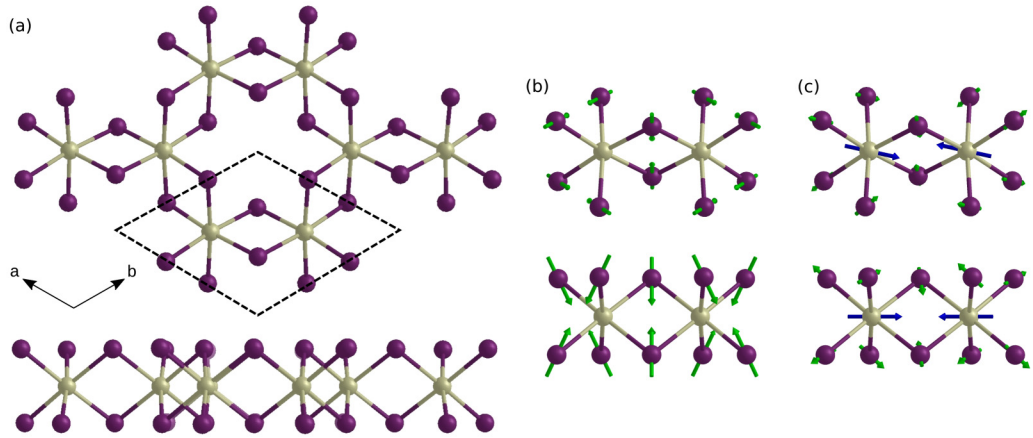

FIG. 1. (a) Top and side views of the crystal structure of single-layer CrI_3. Iodine atoms are purple and chromium atoms are gray. The dashed line shows a 2D primitive unit cell. (b) Top and side views of the A_{1g}^2 mode (110 cm^{-1}) atomic displacements for a single layer of the $R\bar{3}$ structure. Displacements are proportional to the length of the arrow (blue for Cr, green for I). This mode corresponds to an alternate squeezing and spreading of the I layers in the z direction with the Cr layer fixed. (c) E_g^4 (223 cm^{-1}) mode atomic displacements are dominated by alternate in-plane motion of the Cr ions. For the other member of the E_g^4 doublet the Cr ions move in the perpendicular direction within the plane of the layer.

under inversion, while the A_g and A_u modes are even under the C_2 rotation. The 24 modes of the phonon spectrum with C_{2h} symmetry are divided between the irreducible representations as follows:

$$\Gamma_{\text{acoustic}} = A_u + 2B_u, \tag{1}$$

$$\Gamma_{\text{optical}} = 6A_g + 6B_g + 4A_u + 5B_u. \tag{2}$$

For the low-temperature ($R\bar{3}$) structure the point group is $C_{3i} = S_6$, which has two 1-dimensional irreducible representations A_g and A_u and two 2-dimensional irreducible representations E_g and E_u, each describing a pair of degenerate modes. The phonon spectrum with C_{3i} symmetry has the following representations:

$$\Gamma_{\text{acoustic}} = A_u + E_u, \tag{3}$$

$$\Gamma_{\text{optical}} = 4A_g + 4E_g + 3A_u + 3E_u. \tag{4}$$

As the sample thickness decreases, the differences between the phonon spectra of the two structures will decrease. In fact, the single layer of both structures has a higher point symmetry than the bulk, namely, D_{3d}, most likely corresponding to the space group $R\bar{3}2/m$ (No. 166). The D_{3d} point group has the following irreducible representations:

$$\Gamma_{\text{acoustic}} = A_{2u} + E_u, \tag{5}$$

$$\Gamma_{\text{optical}} = 2A_{1g} + 2A_{2g} + 4E_g + A_{1u} + 2A_{2u} + 3E_u. \tag{6}$$

The symmetries of the Raman tensor can be used to predict which modes will be active and with what polarization. The typical experimental setup is a backscattering geometry where the incident light can be plane polarized parallel to the surface of the sample and the scattered light is measured through another polarizer that is either parallel or perpendicular to the incident polarization. We consider measurements with the incident light normal to the CrI_3 layers. All Raman-active modes must be inversion symmetric (''g'' modes). The results of the first-principles calculations of the phonon spectrum of CrI_3, including the polarization dependence, are shown in Table I. As expected, the results from the two calculations of the single-layer spectrum are quite similar. All frequencies of

TABLE I. Calculated optical phonon frequencies ω_{opt}, in cm^{-1}, and assignment to irreducible representations of C_{3i}, the point group for the $R\bar{3}$ structure; C_{2h}, the point group of the $C2/m$ structure; and D_{3d}, the point group of the single-layer structure. Bold values correspond to Raman-active modes for parallel (∥) and perpendicular (⊥) configurations of incident and scattered radiation.

$R\bar{3}$ structure				$C2/m$ structure		
C_{3i}	Bulk ω_{opt}	Single layer ω_{opt}	D_{3d}	Single layer ω_{opt}	Bulk ω_{opt}	C_{2h}
A_u	240	245	A_{2u}	246	242	B_u
E_g	∥, ⊥ **225**	∥, ⊥ **223**	E_g	∥, ⊥ **225**	225	B_g
	∥, ⊥ **225**	∥, ⊥ **223**		∥, ⊥ **225**	∥ **224**	A_g
E_u	206	205	E_u	207	206	B_u
	206	205		207	206	A_u
A_g	∥ **195**	195	A_{2g}	196	196	B_g
A_g	∥ **125**	∥ **119**	A_{1g}	∥ **120**	∥ **125**	A_g
A_u	123	122	A_{1u}	123	124	A_u
E_u	107	105	E_u	106	108	A_u
	107	105		106	107	B_u
E_g	∥, ⊥ **102**	∥, ⊥ **99**	E_g	∥, ⊥ **100**	∥ **102**	A_g
	∥, ⊥ **102**	∥, ⊥ **99**		∥, ⊥ **100**	101	B_g
E_g	∥, ⊥ **98**	∥, ⊥ **96**	E_g	∥, ⊥ **96**	∥ **99**	A_g
	∥, ⊥ **98**	∥, ⊥ **96**		∥, ⊥ **96**	99	B_g
A_g	∥ **88**	86	A_{2g}	87	⊥ **86**	B_g
E_u	83	76	E_u	77	82	A_u
	83	76		77	79	B_u
A_g	∥ **79**	∥ **75**	A_{1g}	∥ **76**	∥ **79**	A_g
A_u	64	58	A_{2u}	59	58	B_u
E_g	∥, ⊥ **53**	∥, ⊥ **48**	E_g	∥, ⊥ **48**	52	B_g
	∥, ⊥ **53**	∥, ⊥ **48**		∥, ⊥ **48**	∥ **51**	A_g

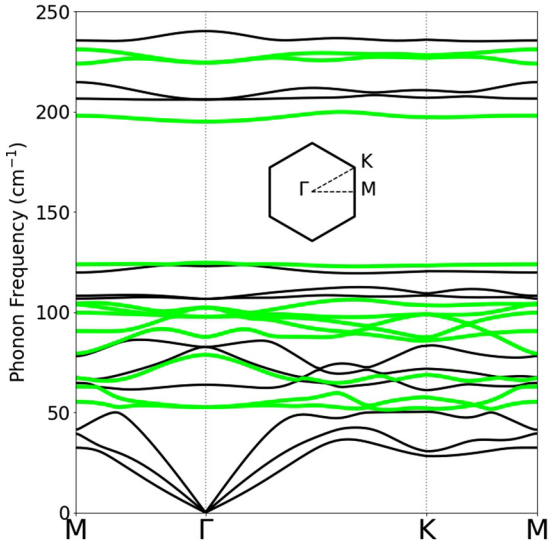

FIG. 2. Phonon band structure for the bulk $R\bar{3}$ structure along a path from M to Γ to K to M in the two-dimensional Brillouin zone, shown in the inset. Colored bands show those modes expected to be Raman active at Γ.

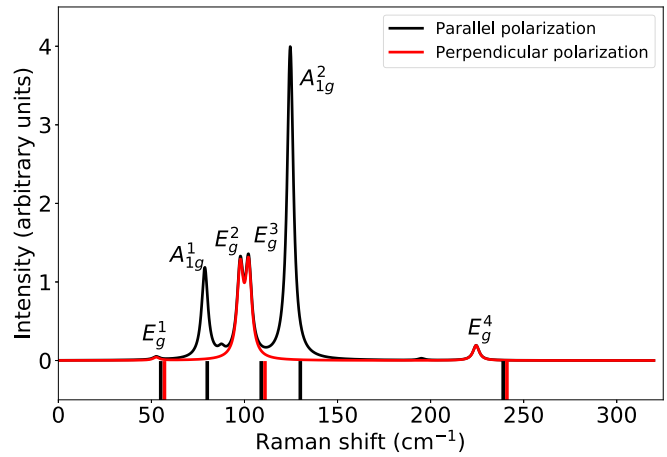

FIG. 3. Raman spectrum for bulk $R\bar{3}$ CrI_3 labeled with D_{3d} irreducible representations for the active modes for parallel (black) and perpendicular (red) polarization. The peaks have been broadened by a Lorentzian with FWHM 4 cm^{-1}. The vertical lines beneath the spectrum show the locations of the major peaks in the measured Raman spectrum [13].

the single-layer $R\bar{3}$ structure are slightly lower than those of the corresponding modes in the single-layer $C2/m$ structure, but none by more than 2%.

The bulk $C2/m$ spectrum displays near degeneracy between several pairs of A and B modes. By comparing to the single-layer and $R\bar{3}$ spectra, we see that they match the E modes of the C_{3i} and D_{3d} point groups. This implies that the symmetry breaking in the $C2/m$ structure due to the layer stacking is not very strong, as one might expect for weak van der Waals coupling between the layers.

In Figs. 1(b) and 1(c) we show the atomic displacements for the two modes with largest measured intensity. In Fig. 2 we show the phonon frequencies along high-symmetry directions of the Brillouin zone for the bulk $R\bar{3}$ structure. Modes that are Raman active at the Γ point are indicated in color. The phonon modes for the $C2/m$ structure are very similar (almost indistinguishable on the scale of this plot). It is interesting to note that the Raman-active modes for the single-layer structure are shifted to lower frequency as compared to the corresponding bulk modes.

We calculate the Raman tensor by taking a finite difference of the macroscopic dielectric tensors for unit cells that have been displaced in the positive and negative direction of each phonon mode. The intensity of the Raman peaks with different polarizations are proportional to the squared magnitude of various components of the Raman tensor. Figure 3 shows the calculated Raman peaks for a bulk $R\bar{3}$ structure (low temperature) for both parallel and perpendicular polarizations. The peaks have been labeled with the appropriate D_{3d} representations. The vertical lines beneath the theoretical spectrum indicate the locations of the experimentally measured Raman peaks from a sample of CrI_3 at $T = 5$ K [13]. Comparison with measured peaks shows that all the predicted peaks are present and that the A_{1g} peaks vanish for perpendicular polarization.

IV. EFFECTS OF MAGNETIZATION, STRAIN, AND INCIDENT ANGLE

One approach to studying the ferromagnetic (FM) phase transition is by comparing the Raman modes from spin-unpolarized, nonmagnetic (NM) calculations with those determined with spin-polarized FM calculations. Within the framework of our calculations, the $R\bar{3}$ FM ground state is lower in energy by 1.53 eV per formula unit compared to the NM state, which is within the range of previously reported values for the NM-FM energy difference, namely, 1.45 [2] and 1.71 eV [3]. The difference in the locations of Raman-active peaks between the NM state and the FM state are shown in Table II. The various modes display a nontrivial pattern of shifts which could be observed in the temperature dependence of the Raman spectrum when passing through the FM transition.

When few- or single-layer materials are stacked or grown on substrates, interactions between layers can cause strain on the atomic structure, leading to changes in the phonon frequencies and observed Raman spectra. To study the effects of strain on CrI_3 we calculate the locations of the Raman peaks for a single layer in the $R\bar{3}$ structure subject to uniform, biaxial strain, induced by increasing or decreasing the lattice constant by up to 10%. All internal coordinates were fully relaxed for each strain configuration. The changes in peak positions are shown in Fig. 4, where the Raman-active modes are color-coded and the spectra for different lattice constants

TABLE II. Difference between ferromagnetic (FM) and nonmagnetic (NM) calculations of optical phonon frequencies (in cm^{-1}) for the Raman-active modes.

Raman mode	E_g^1	A_{1g}^1	E_g^2	E_g^3	A_{1g}^2	E_g^4
$\omega_{\rm opt}$(FM) − $\omega_{\rm opt}$(NM)	10	−1	11	−5	−8	33

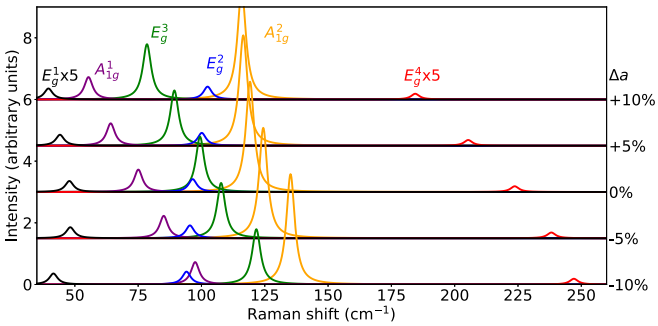

FIG. 4. Change in single-layer $R\bar{3}$ CrI_3 Raman peak locations due to uniform biaxial strain. Peak positions are plotted for changes in the lattice constant (Δa) from -10% to $+10\%$ and offset in the vertical direction for clarity. The peaks have been broadened with a FWHM of 4 cm^{-1}.

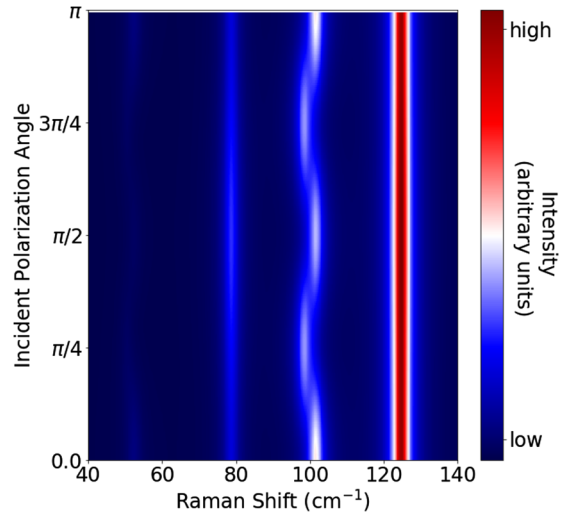

FIG. 5. Dependence of CrI_3 Raman intensity on incident angle for the bulk $C2/m$ structure with parallel polarization. For perpendicular polarization the pattern is the same but the uniform peaks near 80 and 120 cm^{-1} are absent.

are offset in the vertical direction for clarity. While A_{1g}^1, A_{1g}^2, E_g^3, and E_g^4 are all blue shifted with increasing compression (decreasing lattice constant), E_g^2 shows the opposite trend, and E_g^1 changes nonmonotonically. This suggests that the pattern of peaks and their polarization dependence can be used as an indicator of the amount and type of strain experienced by a sample *in situ*.

The Raman intensity is a function of the angle of the incident plane polarization. Our theoretical predictions for the angular dependence in both $R\bar{3}$ and $C2/m$ structures are the following:

(i) There is no discernible angular dependence for the $R\bar{3}$ structure. This occurs because the two degenerate modes within each E_g representation vary oppositely with angle but have the same magnitude and therefore compensate for each other, producing signals that are uniform in the incident angle.

(ii) In the bulk $C2/m$ structure the same modes are not protected by the crystal symmetry and both E_g^2 and E_g^3 representations are split. Within each pair, the two modes are out of phase and have very different magnitudes, which allows the angular dependence of one mode of each pair to dominate. The dominant mode of E_g^2 is also out of phase with the dominant mode of E_g^3, which gives rise to the pattern shown in Fig. 5.

Observation of nontrivial angular dependence in a sample at low temperatures ($R\bar{3}$ structure) would be evidence of another source of symmetry breaking, possibly time-reversal symmetry breaking, due to the ferromagnetic ordering of the spins. A similar effect has been observed in $Cr_2Ge_2Te_6$ [14] and used as evidence for significant spin-phonon coupling. Indeed, the electronic structure of a single layer shows that the calculated magnetization is $3\mu_B$ per Cr ion and exhibits clear ferromagnetic ordering, as shown in Fig. 6, in agreement with previous detailed studies of the magnetic ground state [3–5]. Additionally, including spin-orbit interactions in a noncollinear calculation for the $R\bar{3}$ structure (both bulk and single layer), we find that the orbital moment for each Cr (I) atom is $0.08\mu_B$ ($-0.01\mu_B$), compared to a total magnetic

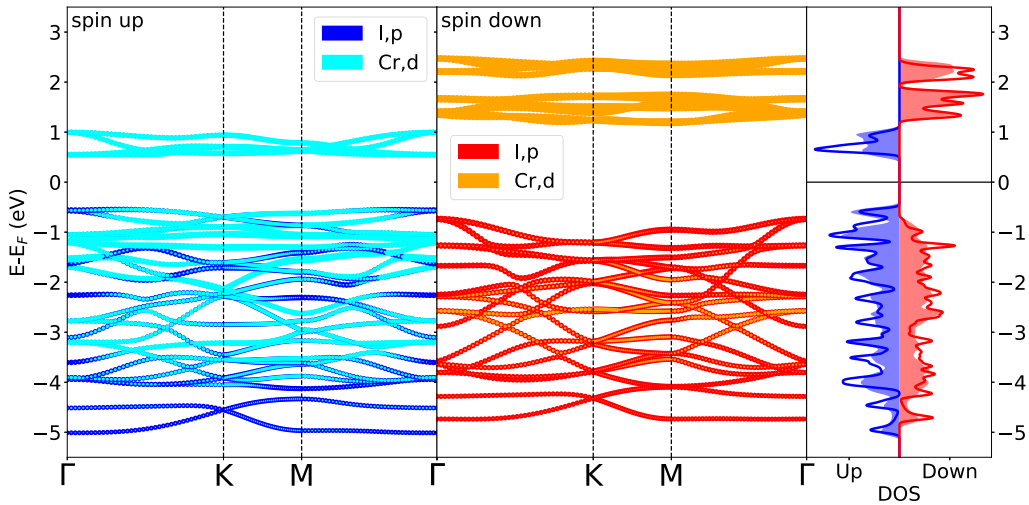

FIG. 6. Orbital character of the electronic bands for the single-layer $C2/m$ structure and DOS for the bulk (shaded regions) and single-layer (solid lines) structures.

moment of $3.1\mu_B$ ($-0.1\mu_B$) for Cr (I). The qualitative features of the density of states (DOS) and band structure are quite similar for bulk and low-temperature structures.

V. CONCLUSION

In conclusion, our calculations of the Raman spectrum of CrI_3 show good agreement with measured locations of the Raman peaks and their polarization dependence. The different amounts by which each mode shifts in response to strain suggests that identifying the shifts in Raman peaks could be a straightforward method for determining strain in experimental samples. The dependence on the incident polarization angle shows that measurements of the angular dependence can be a sensitive probe of symmetry-breaking effects, which might be intimately tied to magnetic ordering.

ACKNOWLEDGMENTS

We thank E. Navarro-Moratalla for helpful discussions about experimental studies of CrI_3 and K. Seyler and X. Xu for sharing with us their Raman measurements. We thank T. D. Rhone for useful discussions about magnetic materials. For the calculations we used the Odyssey cluster supported by the FAS Division of Science, Research Computing Group at Harvard University. We acknowledge partial support from the ARO MURI Award No. W911NF-14-0247.

[1] B. Huang, G. Clark, E. Navarro-Moratalla, D. R. Klein, R. Cheng, K. L. Seyler, D. Zhong, E. Schmidgall, M. A. McGuire, D. H. Cobden *et al.*, Nature (London) **546**, 270 (2017).
[2] H. Wang, V. Eyert, and U. Schwingenschlögl, J. Phys.: Condens. Matter **23**, 116003 (2011).
[3] M. A. McGuire, H. Dixit, V. R. Cooper, and B. C. Sales, Chem. Mater. **27**, 612 (2015).
[4] W.-B. Zhang, Q. Qu, P. Zhu, and C.-H. Lam, J. Mater. Chem. C **3**, 12457 (2015).
[5] J. Liu, Q. Sun, Y. Kawazoe, and P. Jena, Phys. Chem. Chem. Phys. **18**, 8777 (2016).
[6] X. Zhang, Q.-H. Tan, J.-B. Wu, W. Shi, and P.-H. Tan, Nanoscale **8**, 6435 (2016).
[7] G. Kresse and J. Furthmüller, Phys. Rev. B **54**, 11169 (1996).
[8] G. Kresse and J. Furthmüller, Comput. Mater. Sci. **6**, 15 (1996).
[9] J. P. Perdew, K. Burke, and M. Ernzerhof, Phys. Rev. Lett. **77**, 3865 (1996).
[10] S. Grimme, J. Antony, S. Ehrlich, and H. Krieg, J. Chem. Phys. **132**, 154104 (2010).
[11] A. Togo and I. Tanaka, Scr. Mater. **108**, 1 (2015).
[12] A. Fonari and S. Stauffer, *vasp_raman_py* (GitHub, 2013), https://github.com/raman-sc/VASP/.
[13] K. L. Seyler, E. Navarro-Moratalla, and X. Xu (private communication).
[14] Y. Tian, M. J. Gray, H. Ji, R. Cava, and K. S. Burch, 2D Mater. **3**, 025035 (2016).